Electronic Supplementary Material (ESI) for Nanoscale.
This journal is © The Royal Society of Chemistry 2014

Supporting Information for

Kinetically-controlled growth of cubic and octahedral Rh-Pd alloy oxygen reduction electrocatalysts with high activity and durability

Yucong Yan,[a,§] Fangwei Zhan,[a,§] Jingshan Du,[a] Yingying Jiang,[a] Chuanhong Jin,[a] Maoshen Fu,[b] Hui Zhang,[a,] and Deren Yang[a]*

[a]State Key Laboratory of Silicon Materials, Department of Materials Science and Engineering, Key Laboratory of Advanced Materials and Applications for Batteries of Zhejiang Province, and Cyrus Tang Center for Sensor Materials and Applications, Zhejiang University, Hangzhou, Zhejiang 310027, P. R. China.

[b]Shaanxi Materials Analysis and Research Center, School of Materials Science and Engineering, Northwestern Polytechnical University, Xi'an, Shaanxi 710072, P. R. China.

[*]*To whom correspondence should be addressed. E-mail: msezhanghui@zju.edu.cn*

[§]*These authors contributed equally to this work*

Table S1. The productivity of the cube and octahedron in the samples that were prepared by varying the Rh/Pd molar ratios at 140 and 120 ^{o}C, respectively. These data were obtained from about 100 nanocrystals randomly selected from TEM images.

The Rh/Pd molar ratio at 140 ^{o}C	The productivity of cube or octahedron	The Rh/Pd molar ratio at 120 ^{o}C	The productivity of cube or octahedron
4:1	87% cube	4:1	90% cube
2:1	83% cube	2:1	81% cube
1:2	70% octahedron	1:2	84% octahedron
1:4	69% octahedron	1:4	75% octahedron

Table S2. Comparison of feeding ratio of Rh/Pd salt precursors with their atomic ratio in the alloy that achieved from XPS analysis. The XPS spectra were shown in Figure S5.

Feeding ratio of Rh to Pd salt precursor at 120 ^{o}C	Atomic ratio of Rh/Pd at 120 ^{o}C from XPS analysis
Rh/Pd=4:1	Rh/Pd=77:23
Rh/Pd=2:1	Rh/Pd=66:34
Rh/Pd=1:1	Rh/Pd=50:50
Rh/Pd=1:2	Rh/Pd=28:72
Rh/Pd=1:4	Rh/Pd=19:81

Table S3. ECSA, Area, and Mass Activities of Rh-Pd/C towards ORR.*

Samples	**ECSA (m^2/g_{Pt})**	**i_s ($mA/cm^2_{PGM\_Hupd}$)**	**i_m ($mA/\mu g_{PGM}$)**	**i_m ($mA/\mu g_{Pt}$)**
$Rh_{80}Pd_{20}$ cube	6.2	0.15	0.010	0.013
$Rh_{62}Pd_{38}$ cube	16.2	0.04	0.006	0.010
$Rh_{43}Pd_{57}$ octahedron	40.5	0.03	0.011	0.017
$Rh_{29}Pd_{71}$ octahedron	28.3	0.19	0.055	0.092
$Rh_{8}Pd_{92}$ octahedron	42.7	0.24	0.101	0.180

*: The activity was measured at 0.9 V (vs. RHE). All the data are tested for three times and treated without iR compensation.

Table S4. A summary for activity and stability of Pd and Pd-based alloys towards ORR

Samples	**Electrolyte**	**Specific activity (mA/cm^2)**	**Mass activity (mA/μg)**	**Stability**	**Reference**
Rh_8Pd_{92} Octa	0.1 M $HClO_4$	0.24	0.10	Loss 24.7% mass activity or 7 mV of half wave potentials after 30,000 cycles	our work
Pd Cube	0.1 M $HClO_4$	0.31	/	Loss 70% mass activity after 5,000 cycles	1
Pd Octa	0.1 M $HClO_4$	0.03	/	/	2
CoPd NPs	0.1 M $HClO_4$	0.20	0.15	Loss 19 mV of half wave potentials after 5,000 cycles	3
CuPd Cube	0.1 M H_2SO_4	0.31	0.13	/	4
$Rh_{20}Pd_{80}$ Nanodendrites	0.1M KOH	/	0.26[a]	Loss 24.7% mass activity after 10,000 cycles	5

a:this data was obtained at 0.8 V.

References

1. M. Shao, J. Odell, M. Humbert, T. Yu and Y. Xia, *J. Phys. Chem. C*, **2013**, 117, 4172-4180.
2. M. Shao, T. Yu, J. Odell, M. Jin and Y. Xia, *Chem. Commun.*, **2011**, 47, 6566-6568.
3. C. Xu, Y. Liu, H. Zhang and H. Geng, *Chem. Asian J.* **2013**, 8, 2721-2728.
4. L. Zhang, F. Hou and Y. Tan, *Chem. Commun.*, **2012**, 48, 7152-7154.
5. Y. Qi, J. Wu, H. Zhang, Y. Jiang, C. Jin, M. Fu, H. Yang and D. Yang, *Nanoscale*, **2014**, 6, 7012-7018.

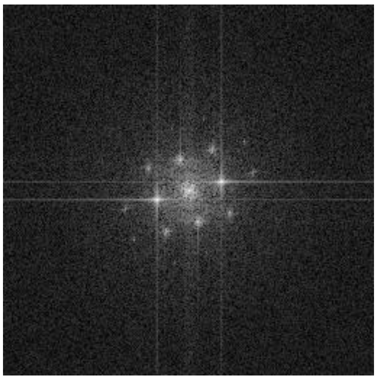

Figure S1. Fourier transform (FFT) pattern of a single Rh-Pd alloy nanocubes in Figure 2C.

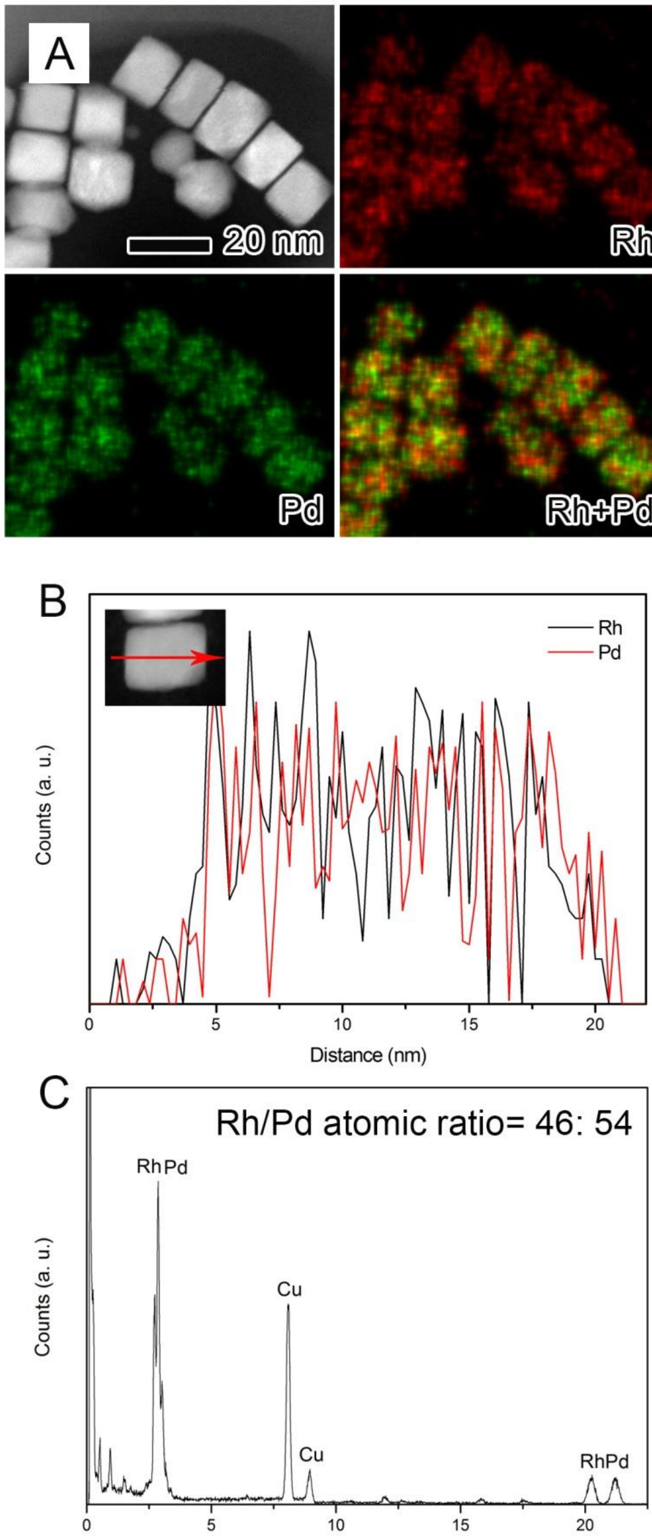

Figure S2. (A) HAADF-STEM-EDX mapping, (B) EDX line-scan profile, and (C) EDX spectrum of Rh-Pd alloy nanocubes prepared using the standard procedure.

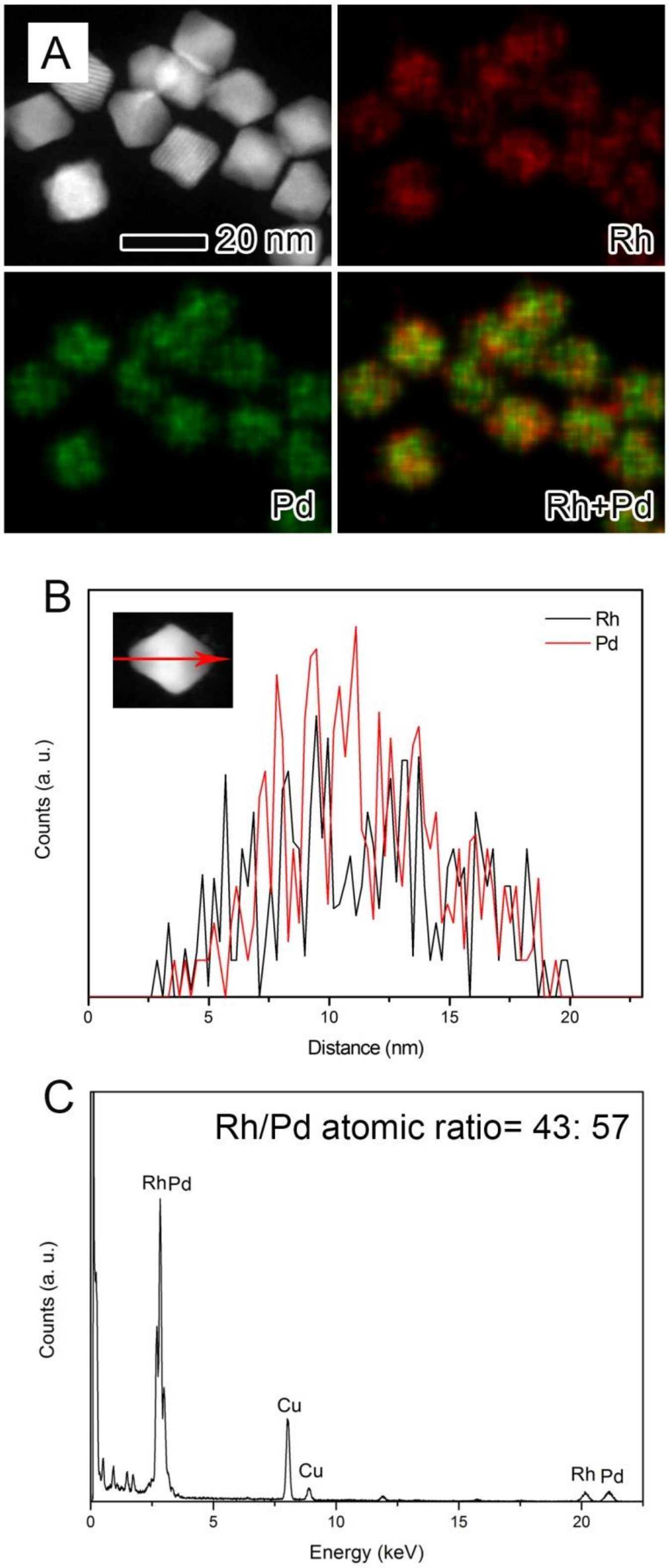

Figure S3. (A) HAADF-STEM-EDX mapping, (B) EDX line-scan profile, (C) EDX spectrum of Rh-Pd alloy octahedra prepared using the standard procedure except for the different reaction temperature at 120 ^{o}C.

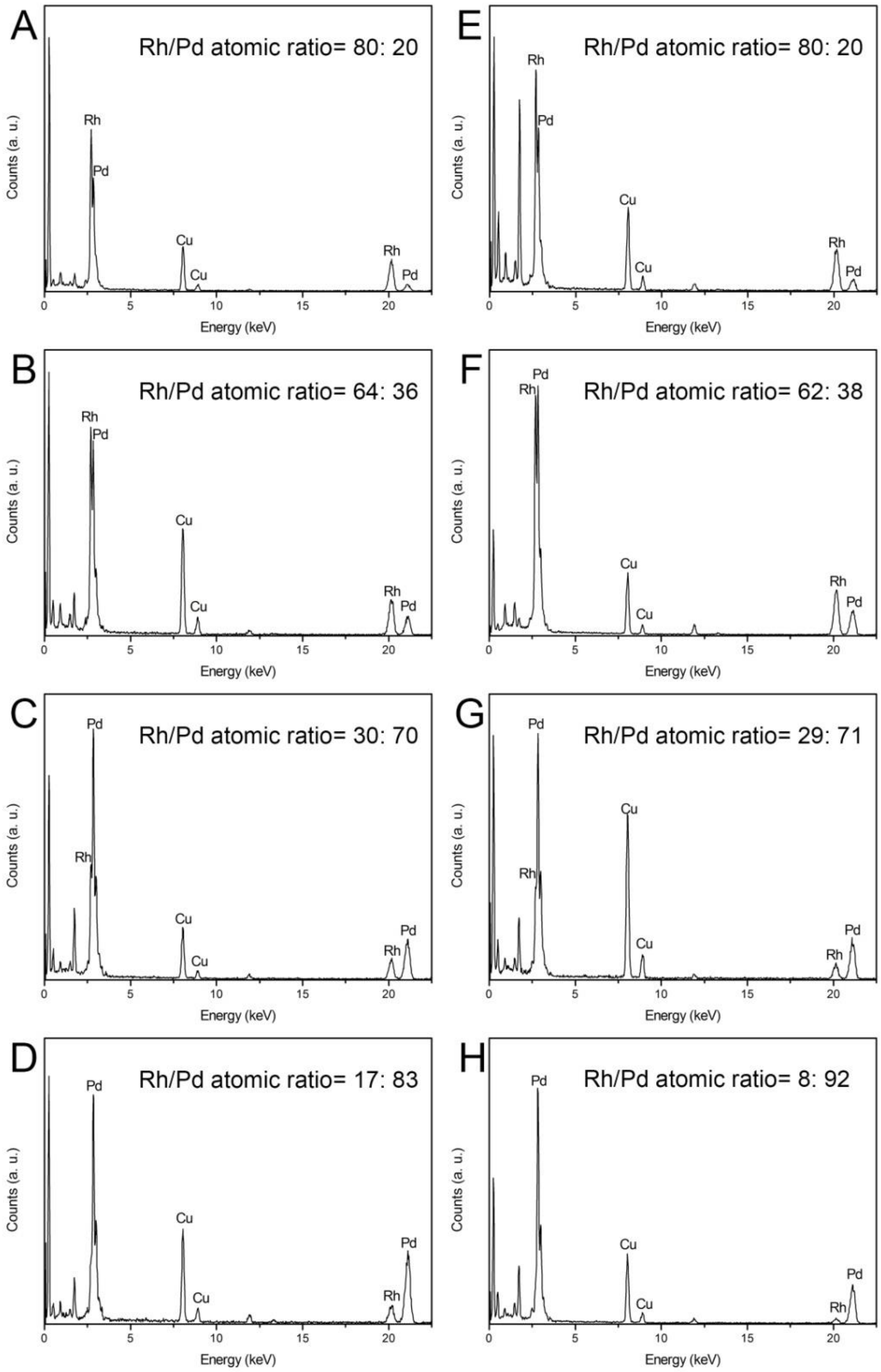

Figure S4. EDX spectra of Rh-Pd alloy nanocrystals that were obtained at 140 (A-D) and 120 ^{o}C (E-H), respectively, by varying the Rh/Pd molar ratios: (A, E) 4:1, (B, F) 2:1, (C, G) 1:2, and (D, H) 1:4.

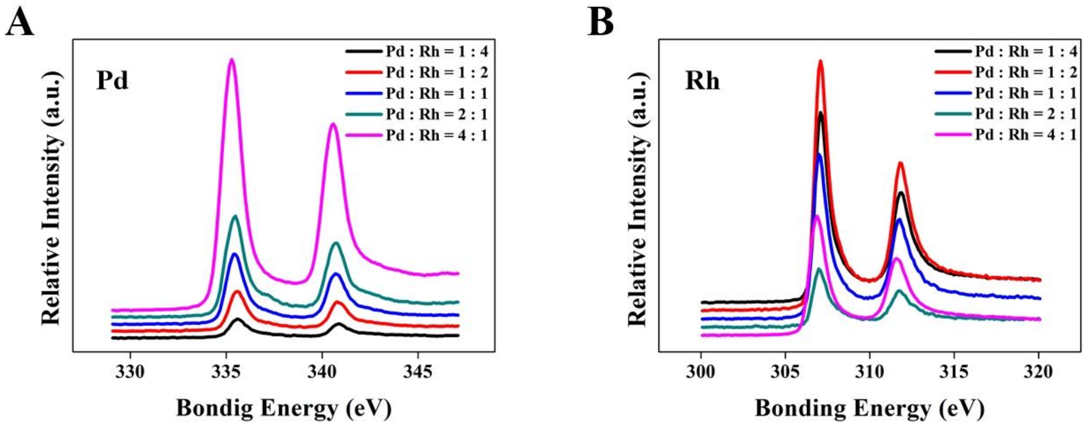

Figure S5. XPS spectra of the Rh-Pd alloy nanocrystals with different compositions prepared at 120 ^{o}C.

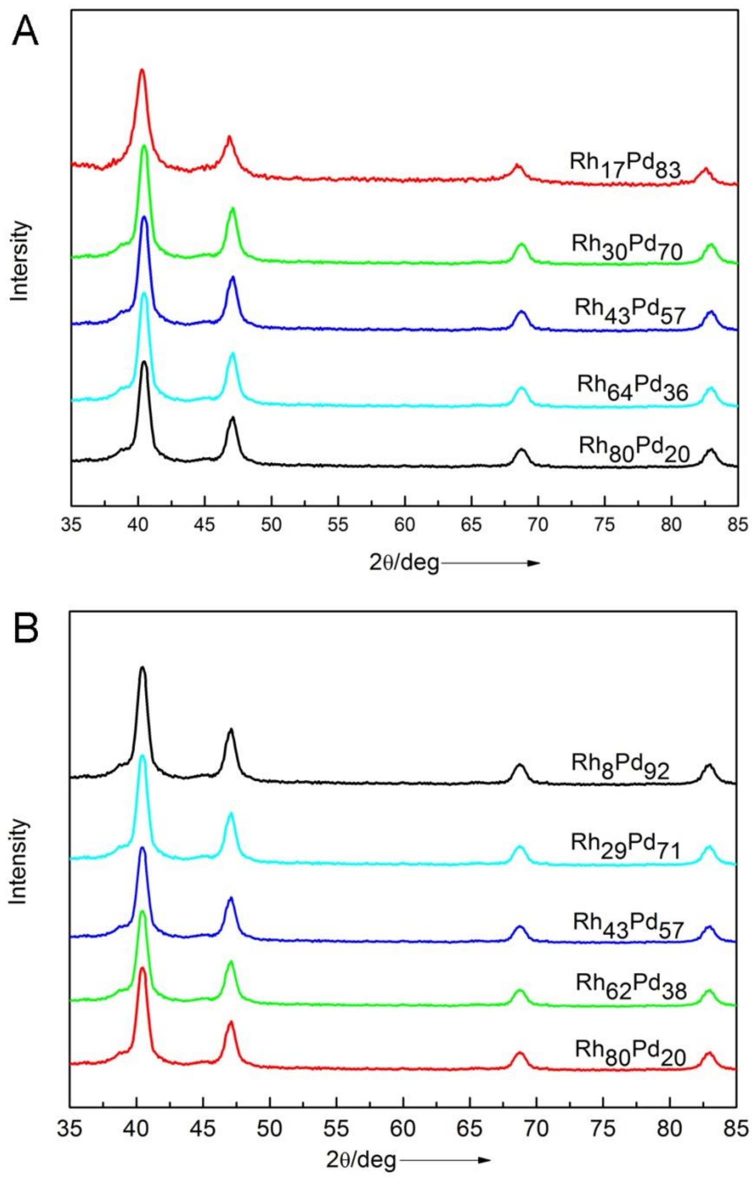

Figure S6. XRD patterns of Rh-Pd alloy nanocrystals with different compositions that prepared at different temperature: (A) 140 and (B) 120 ^{o}C.

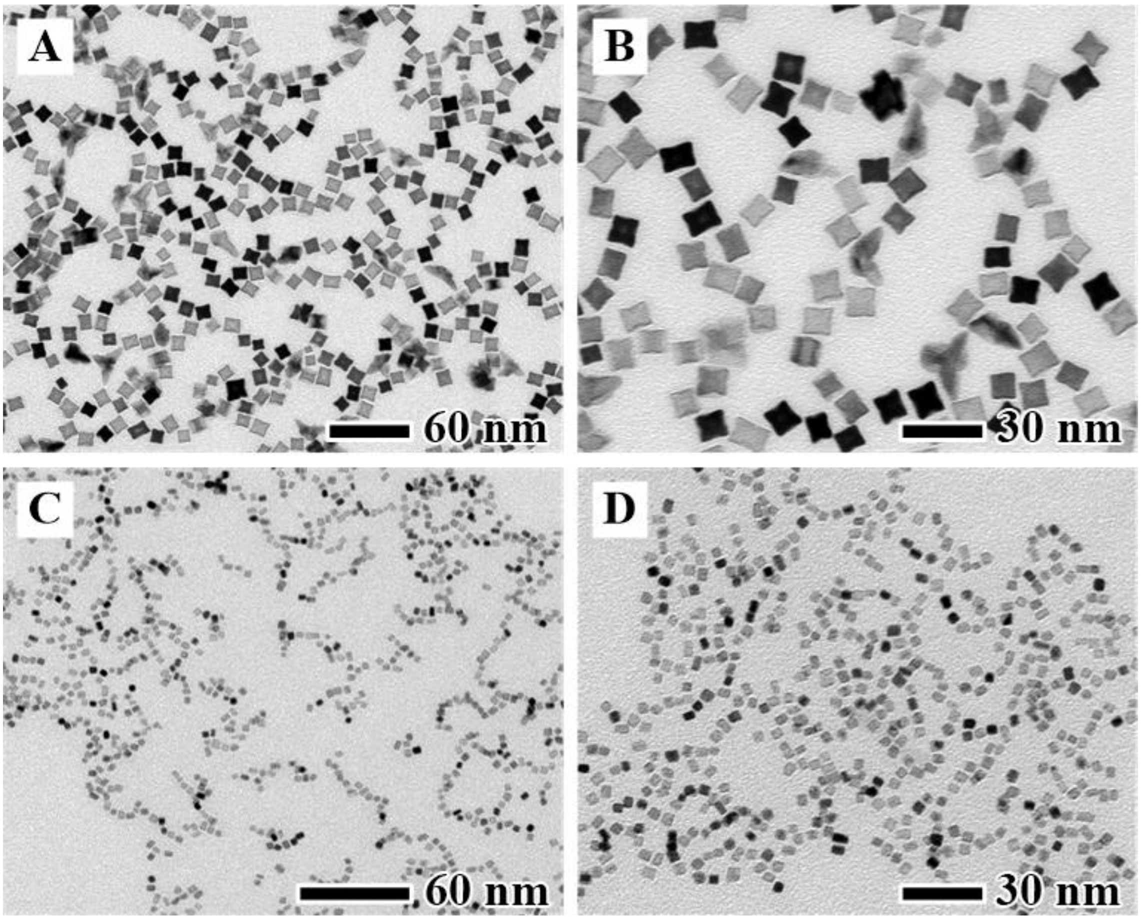

Figure S7. TEM images of Rh nanocrystals that prepared by reducing Na_3RhCl_6 with AA in EG at different injection rate at 140 ^oC: (A, B) 2 mL/h and (C, D) *ca.* 2.5 mL/s using a pipette.

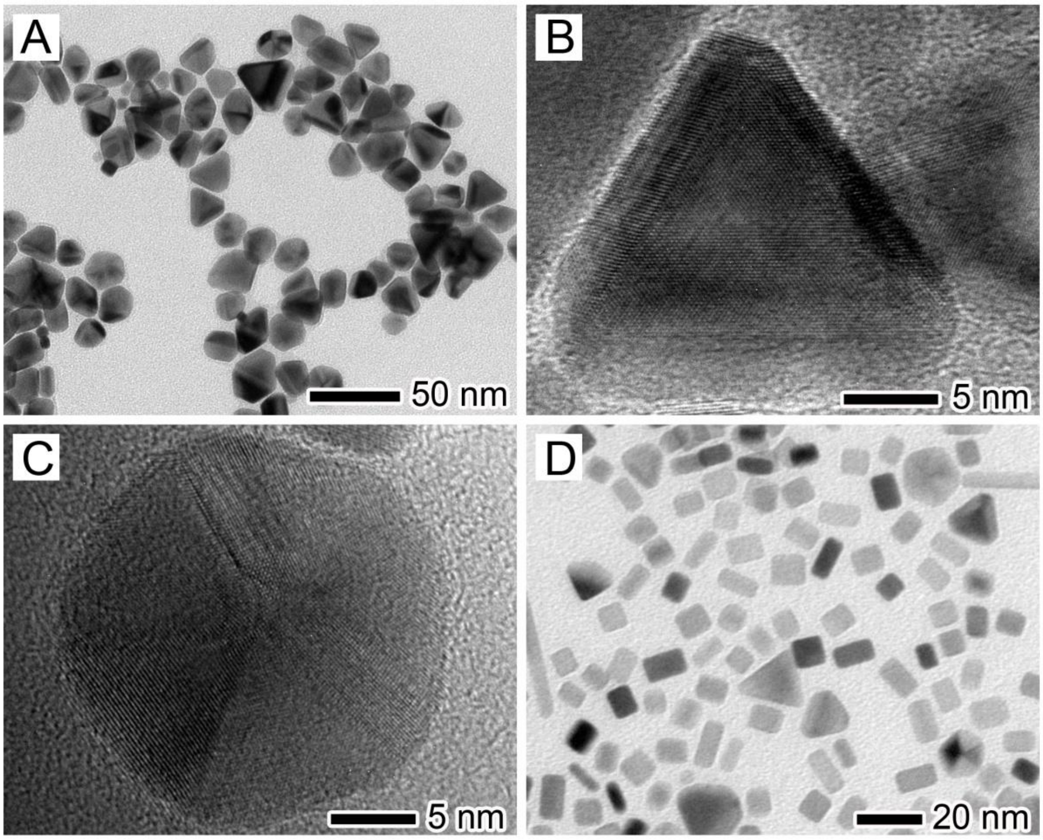

Figure S8. (A) TEM and (B, C) HRTEM images of Pd nanocrystals that were prepared by injecting Na_2PdCl_4 with a rate of 2 mL/h using a syringe pump into ethylene glycol containing ascorbic acid and KBr at 140 ^oC. (D) TEM image of Pd nanocrystals that were prepared using the similar approach, except for the injection of Na_2PdCl_4 with pipette (*ca.* 2.5 mL/s).

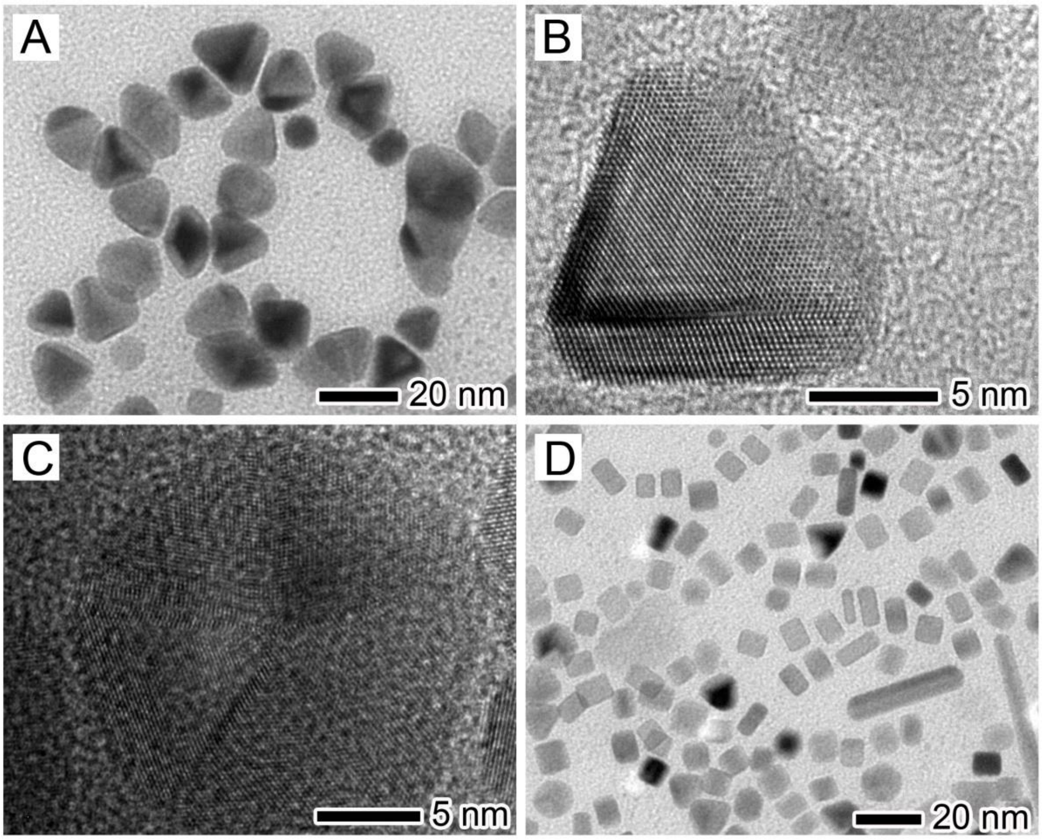

Figure S9. (A) TEM and (B, C) HRTEM images of Pd nanocrystals that were prepared by injecting Na_2PdCl_4 with a rate of 2 mL/h using a syringe pump into ethylene glycol containing ascorbic acid and KBr at 120 ^oC. (D) TEM image of Pd nanocrystals that were prepared using the similar approach, except for the injection of Na_2PdCl_4 with pipette (*ca.* 2.5 mL/s).

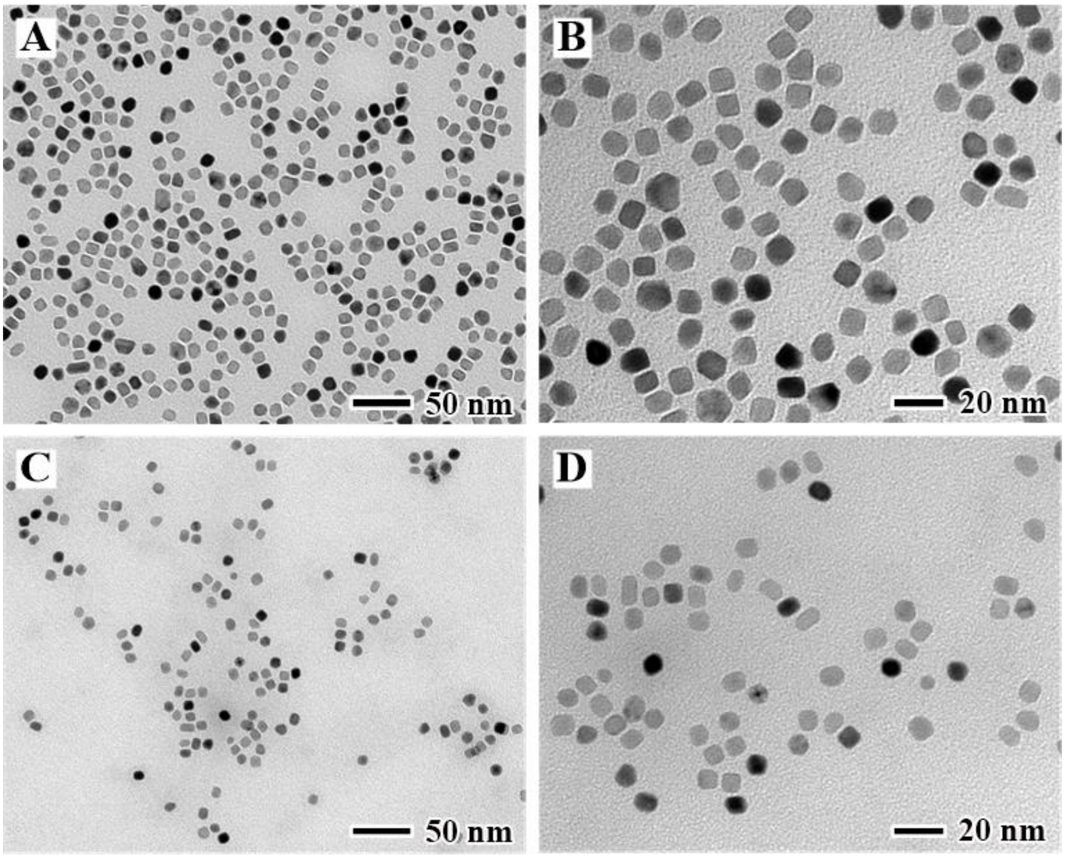

Figure S10. TEM images of the Rh-Pd alloy nanocrystals that prepared at 120 ^{o}C with an injection rate of 0.5 mL/min by varying the Rh/Pd molar ratios: (A, B) 1:2 and (C, D) 1:4.

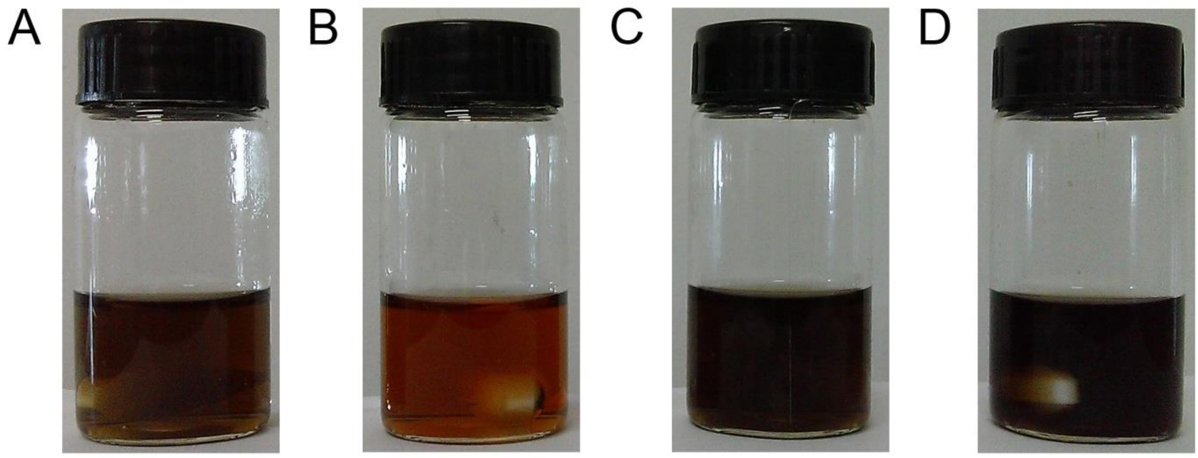

Figure S11. Photographs of the samples that were prepared by adding 0.5 mL of a precursor into 6 mL of ethylene glycol containing ascorbic acid and KBr at different temperature and lasting for 5 min: (A) Na_3RhCl_6 at 120 ^oC, (B) Na_2PdCl_4 at 120 ^oC, (C) Na_3RhCl_6 at 140 ^oC, and (D) Na_2PdCl_4 at 140 ^oC.

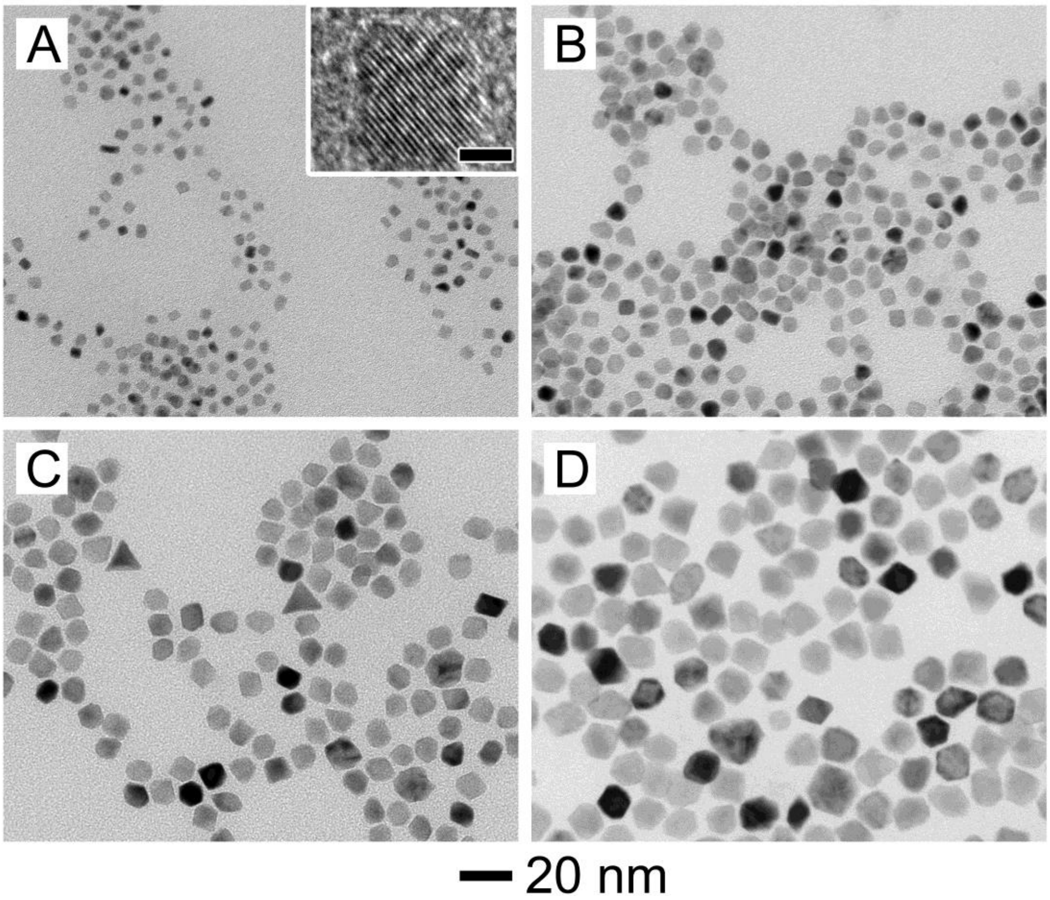

Figure S12. TEM images of the samples that were prepared using the standard procedure, except for the different period of times reacting at 120 ^{o}C: (A) 15 min, (B) 30 min, (C) 1 h, and (D) 2 h. The inset shows HRTEM image of an individual cube in (A). The scale bar in the inset is 2 nm.

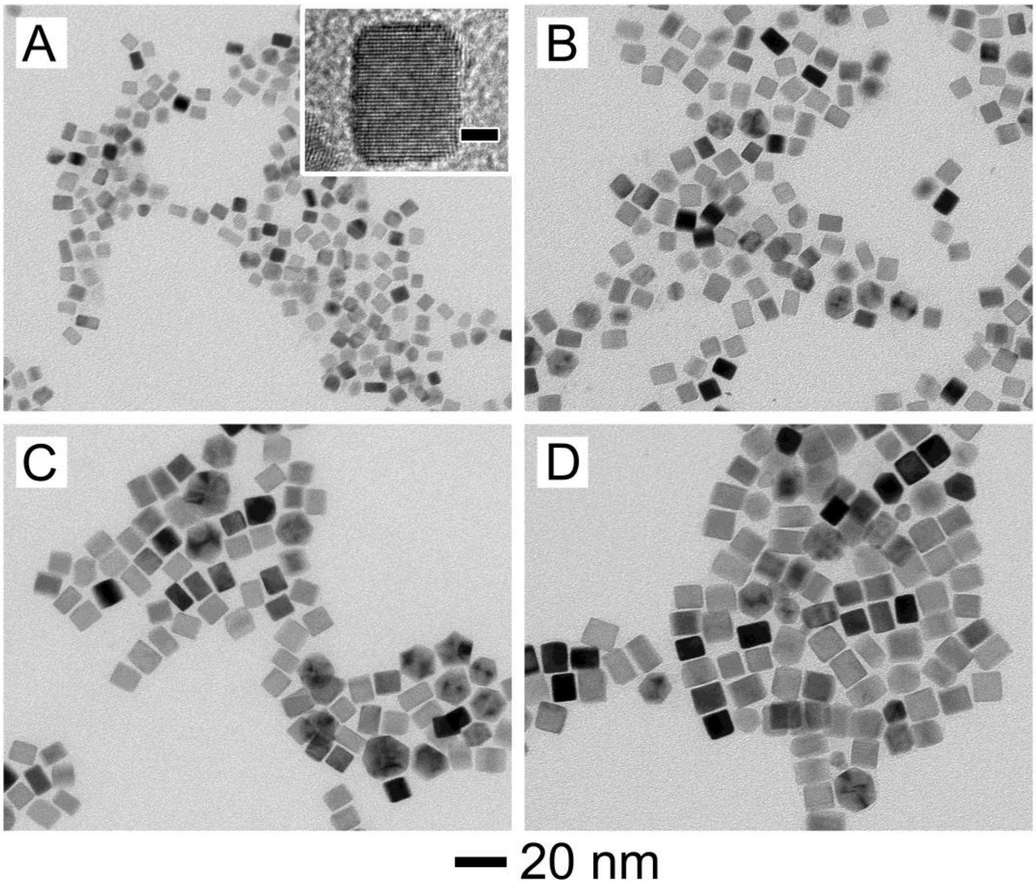

Figure S13. TEM images of the samples that were prepared using the standard procedure, except for the different period of times: (A) 15 min, (B) 30 min, (C) 1 h, and (D) 2 h. The inset shows HRTEM image of an individual cube in (A). The scale bar in the inset is 2 nm.

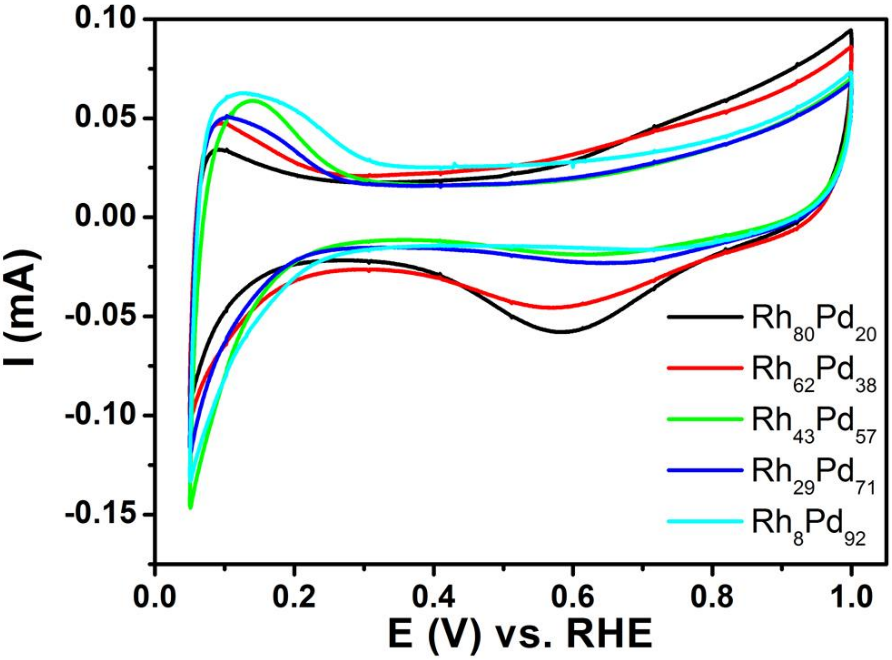

Figure S14. CV curves of Rh-Pd catalysts made at 120 ^{o}C.

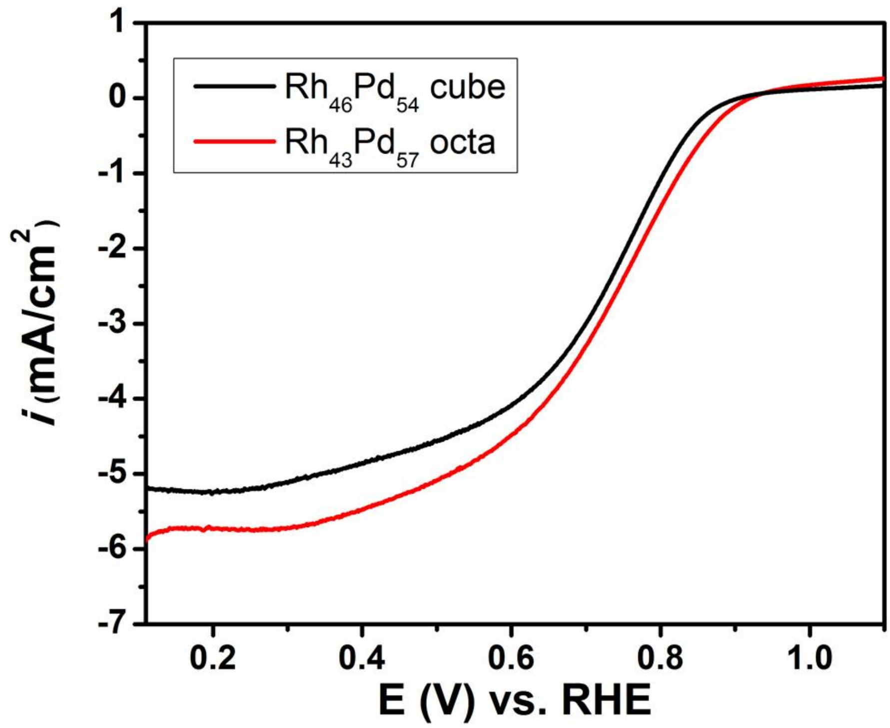

Figure S15. ORR polarization curves of cubic $Rh_{46}Pd_{54}$ and octahedral $Rh_{43}Pd_{57}$ catalysts made at 140 and 120 ^{o}C, respectively.

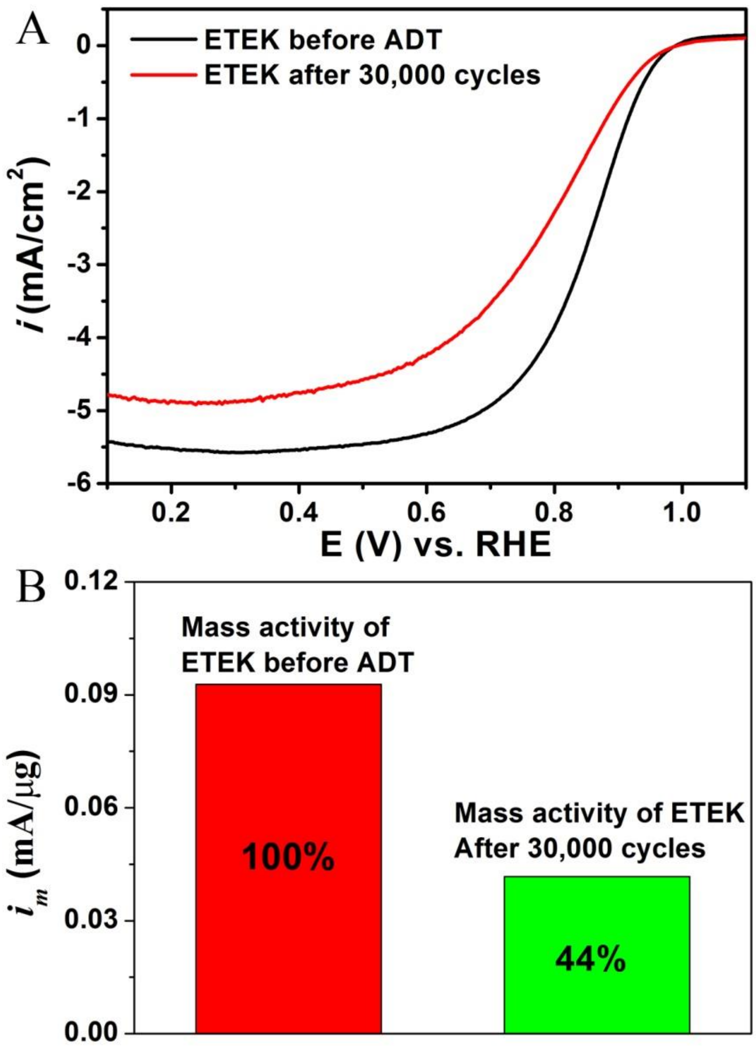

Figure S16. (A) ORR polarization curves and (B) mass activities of the commercial Pt/C (ETEK) before and after ADT test. The test condition is the same as that for the Rh-Pd based catalysts.

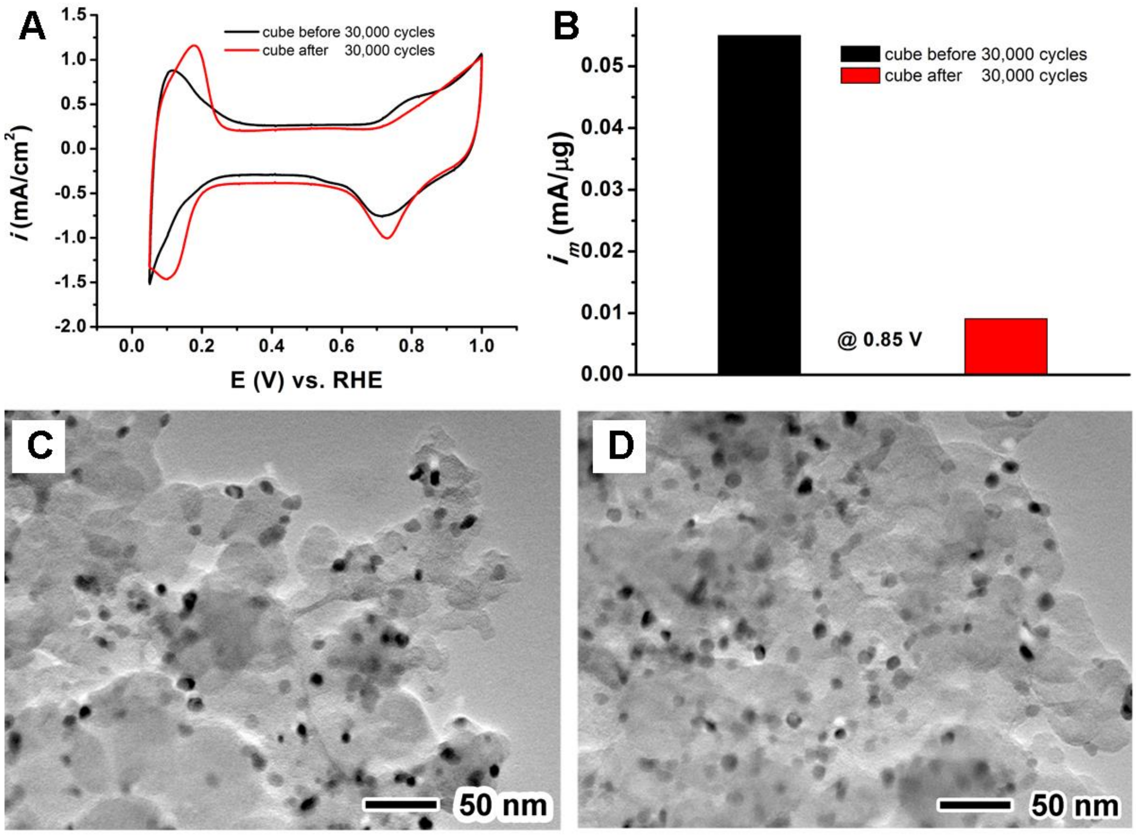

Figure S17. (A) CV curves and (B) mass activities of carbon supported Pd nanocubes before and after ADT test. (C, D) TEM images of carbon supported Pd nanocubes after ADT test.

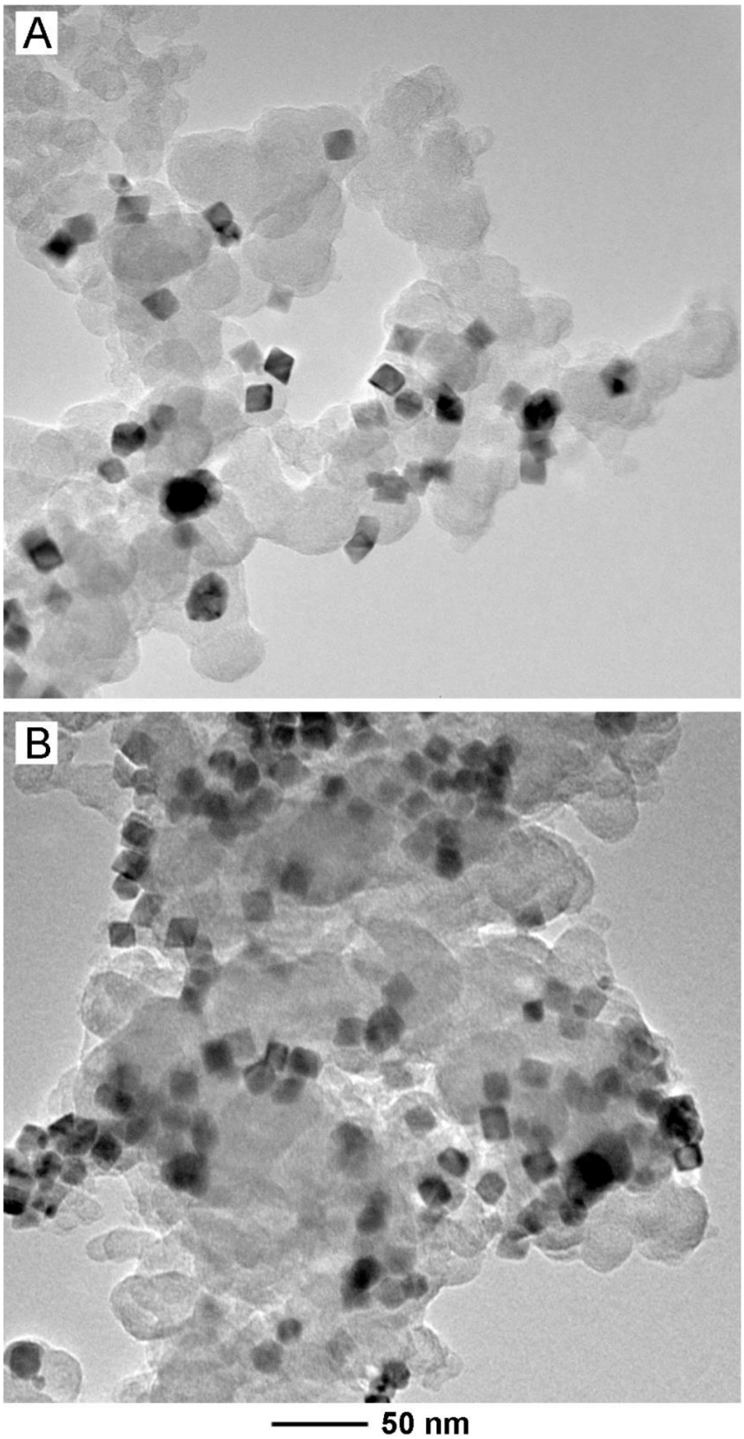

Figure S18. TEM images of carbon supported Rh_8Pd_{92} octahedrons after ADT test for 30,000 cycles.